Broadband near-field radiative thermal emitter/absorber based on hyperbolic metamaterials: Direct numerical simulation by the Wiener chaos expansion method

Baoan Liu and Sheng Shen

Phys. Rev. B **87**, 115403 — Published 4 March 2013

DOI: 10.1103/PhysRevB.87.115403

Broadband near-field radiative thermal emitter/absorber based on hyperbolic metamaterials: Direct numerical simulation by Wiener-chaos expansion methods

Baoan Liu, Sheng Shen*
Department of Mechanical Engineering, Carnegie Mellon University, Pittsburgh, PA, 15213, USA

PACS numbers: 44.40.+a, 81.05.Xj

*Corresponding author. E-mail: sshen1@cmu.edu

Abstract

In the near-field, radiative heat transfer can exceed the prediction from Planck's law by several orders of magnitude, when the interacting materials support surface polaritons in the infrared range. However, if the emitter and absorber are made from two different materials, which support surface polariton resonances at different frequencies, the mismatch between surface polariton resonance frequencies will drastically reduce near-field radiative heat transfer. Here, we present a broadband near-field thermal emitter/absorber based on hyperbolic metamaterials, which can significantly enhance near-field radiative heat transfer with infrared surface-polariton-resonance materials and maintain the monochromatic characteristic of heat transfer. Instead of using effective medium approximation, we perform a direct numerical simulation to accurately investigate the heat transfer mechanisms of metamaterials based on the Wiener-chaos expansion method.

I. Introduction

In the near-field, when the gap distance between objects is smaller than the dominant thermal wavelength predicted by Wien's displacement law, radiative heat transfer can be greatly enhanced by photon tunneling through evanescent electromagnetic waves[1–3]. In particular, it has been demonstrated that near-field radiative heat transfer can exceed the prediction from Planck's law by several orders of magnitude[4–6], when the interacting materials support infrared surface-polariton resonances (IR-SPRs), including surface phonon polaritons in polar dielectric materials[4] (e.g., cBN, SiC or SiO_2) and surface plasmon polaritons in doped semiconductors[7]. In contrast to far-field radiation in which the spectral distribution of emissive power is usually broadband, near-field thermal emission from an IR-SPR material is almost monochromatic[8]. The IR-SPR based near-field radiation is practically important due to the significant heat transfer enhancement and quasi-monochromatic emission, and has been suggested to be used to increase the efficiency of thermophotovoltaic devices[9,10] and create vacuum thermal rectifiers[11,12].

However, the IR-SPR based near-field heat transfer is strongly material-dependent. The enhancement of heat transfer between two identical IR-SPR materials arises from the coupling of surface polariton waves[8]. If the emitter and absorber are made from different materials which support SPRs at different frequencies, the mismatch between SPR frequencies will result in much less heat transfer. For instance, SiC supports surface phonon polaritons in the infrared range, but gold supports surface plasmon polaritons in the visible range. As shown in Fig. 1, near-field radiative heat transfer between semi-infinite SiC and gold plates is found to be three orders of magnitude less than that between two SiC plates.

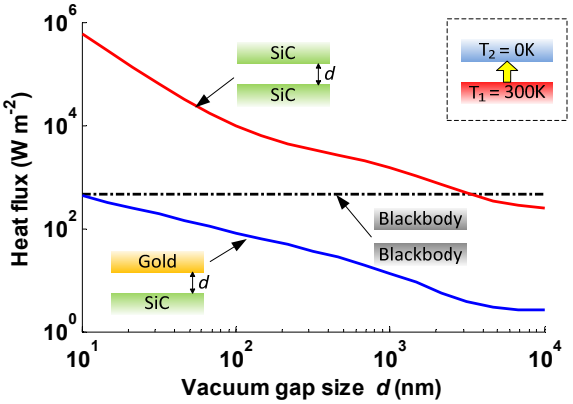

FIG.1: (color online). Plot of radiative heat transfer between two semi-infinite plates maintained at 0K

and 300K against the vacuum gap size d . SiC-SiC case (red curve) is compared with SiC-gold case (blue curve). Blackbody radiation limit is also plotted for reference (black dashed line).

To overcome the material limitation of the IR-SPR based near-field radiation, "metamaterials" have been proposed to enhance near-field radiative heat transfer by designing SPRs at desired frequencies[13]. Metamaterials, which are typically structured at a scale smaller than $1/10^{th}$ of wavelength, are artificial composite materials whose electromagnetic properties are engineered by sub-wavelength structures such as split-ring resonators and dilute metal wires[14,15]. If the gold plate in Fig. 1 is replaced by the arrays of sub-wavelength gold wires or split ring resonators, the effective resonant frequency of surface plasmon polaritons in the metamaterial can be shifted to match the resonant frequency of surface phonon polaritons in SiC. However, in order to maintain designed effective properties and manipulate thermal radiation in the near-field, a metamaterial needs to meet two criteria: (i) the feature size of the metamaterial (e.g., period of sub-wavelength structures) must be much smaller than the gap size between the emitter and the absorber, which can be in the range of tens of nanometers[16], and (ii) the metamaterial must have an effective resonant frequency in the infrared range (e.g., wavelength around $10\mu m$) in order to match the resonant frequency of an IR-SPR emitter. For both criteria to be fulfilled simultaneously, the diameters of dilute metal wires and the thicknesses of split ring resonators are predicted to be in the sub-nanometer scale. Although these resonant metamaterials show potential for manipulating near-field radiation, they are very difficult to be experimentally realized with current fabrication technologies.

In this paper, we present a broadband non-resonant heat emitter/absorber based on hyperbolic metamaterials[17–19], which can significantly enhance near-field radiative heat transfer between metals and IR-SPR thermal emitters, and maintain the monochromatic characteristic of the IR-SPR based near-field radiation. In order to elucidate the heat transfer mechanisms of complex three-dimensional metamaterials, we directly calculate near-field radiation based on the Wiener-chaos expansion method, rather than using effective medium theory (EMT). Previous studies on metamaterial based near-field radiation generally adopted EMT to approximate electromagnetic properties[13,20]. However, EMT approximation has two drawbacks: (i) It may not be applicable in the near-field because, instead of effective or averaged properties, inhomogeneous behaviors of individual sub-wavelength structures dominate the responses of metamaterials to the exponentially decaying evanescent waves. (ii) EMT is essentially an approximation which cannot provide detailed information on the electromagnetic fields in metamaterials. A direct numerical simulation is thus crucial for accurately predicting the near-field responses of complicated geometries like metamaterials.

II. Enhanced near-field heat transfer between an IR-SPR emitter and a hyperbolic metamaterial

Hyperbolic metamaterials are non-resonant and can potentially manipulate near-field radiation[17,21]. The effective permittivity of this type of metamaterials has a negative vertical component ($\varepsilon_z < 0$) and positive horizontal components ($\varepsilon_{x,y} > 0$), with the materials assumed to be uniaxial (i.e., $\varepsilon_x = \varepsilon_y = \varepsilon_{x,y}$) for simplicity. Since ε_z and $\varepsilon_{x,y}$ are opposite in sign, the dispersion relation for TM (transverse-magnetic, H_z=0) waves is a hyperbolic function

$$\frac{k_z^2}{\varepsilon_{x,y}} - \frac{K^2}{|\varepsilon_z|} = k_0^2, \qquad (1)$$

where K is the lateral wave vector $K = \sqrt{k_x^2 + k_y^2}$, and k_0 is the wave vector in vacuum. As shown in Eq. (1), one intriguing property of hyperbolic metamaterials is that they allow propagating TM waves with no upper bound for K. The IR-SPR based near-field heat transfer is dominated by the contribution from the TM waves that have a purely imaginary k_z and a large surface wave vector K ($K > k_0$)[1]. These waves are evanescent in vacuum but can be converted into propagating waves by hyperbolic metamaterials for arbitrarily large K.

Hyperbolic metamaterials can be realized by a number of structures such as alternating metal-dielectric layers[17] and metal wire arrays (MWAs)[18,19]. In the infrared regime, metals behave like perfect electric conductors (PEC) with permittivity $\varepsilon = -\infty + i\infty$. A metamaterial made of MWAs can have the hyperbolic dispersion given by Eq. (1) in a broad frequency band for $\omega < \omega_p$ without relying on the intrinsic resonant properties of metals. Here, ω_p is the equivalent plasma frequency of MWAs, which can be expressed by the wire period a and the radius r as $\omega_p \approx \sqrt{2\pi c_0^2 / [a^2 \ln(a/r)]}$ [22]. The vertical components of the effective permittivity $\varepsilon_{x,y}$ can be approximated as the vacuum permittivity ε_0 due to the negligible polarizability in x- or y- direction. However, the estimation of the parallel component ε_z is not straightforward. The local EMT model for "diluted metal wires" proposed by Pendry *et al.* [22] cannot interpret the dispersion of the propagating waves inside the MWAs[18,19]. Belov *et al.*[18] proposed a non-local EMT model for MWAs which requires evaluating the microscopic structure details

$$\varepsilon_z(\omega, k_z) = \varepsilon_0 \left(1 - \frac{\omega_p^2}{\omega^2 - c_0^2 k_z^2} \right), \qquad (2)$$

which is always negative for $\omega < \omega_p$. If the period of MWAs is chosen to be hundreds of nanometers, ω_p of MWAs is typically in the visible range, and MWAs can maintain the hyperbolic dispersion in the infrared range.

The performance of MWAs can be evaluated by the photon local density of states (LDOS) above the surface of semi-infinite MWAs. According to Ref. [23], the photon tunneling rate through evanescent waves increases with the increase of the LDOS immediately above the surface of the thermal emitter/absorber. Therefore, by enhancing the LDOS, near-field radiative heat transfer can be increased. The LDOS, $\rho_i(d, K, \omega)$, at the distance d above the surface of a medium for parallel wave vector K and frequency ω is related by

$$\rho_i(d, K, \omega) \propto \mathrm{Im}[r_{TM}^i]\exp(-\gamma d), \qquad (3)$$

where r_{TM}^i is the Fresnel factor of the medium i$\in$ {emitter, absorber} for TM waves, and $\gamma = \sqrt{k_0^2 - K^2}$. Here, we ignore the contribution from the transverse-electric (TE) wave since the near-field heat transfer with an IR-SPR emitter is dominated by TM waves. Furthermore, the profile of the spectral heat flux $\Phi(\omega)$ between a thermal emitter and absorber separated by a vacuum gap d can be estimated by the product of the LDOS above the surface of each individual medium

$$\int_{k_0}^{\infty} d^2K \cdot \rho_{emitter}(d, K, \omega) \cdot \rho_{absorber}(d, K, \omega). \qquad (4)$$

Due to the hyperbolic dispersion, the LDOS above MWAs can be dramatically increased compared to that of bulk metals. However, the exact value of the LDOS of MWAs is difficult to be calculated based on the non-local EMT model (Eq. (2)), because the calculation of the Fresnel factors of non-local media requires to scrutinize the structure details[24]. Hence, we consider a limiting case with local dispersion relation to predict the general trend of the LDOS above MWAs. If the period of MWAs is infinitely small, the equivalent plasma frequency approaches infinity, $\omega_p \to \infty$, then the effective permittivity of this limiting case of MWAs is $\varepsilon_x = \varepsilon_y = \varepsilon_0, \varepsilon_z = -\infty$ according to Eq. (2). The limiting case is a reasonable approximation to the actual MWAs in the near-field because it can lead to the same dispersion relation of the propagating waves inside MWAs as that of the actual cases when $\omega < \omega_p$ [18,19]. The LDOS can thus be easily evaluated by calculating the Fresnel factor for an anisotropic medium with local EMT model [16]. In Fig. 2, we estimate the LDOS at 100nm above the surface of the semi-infinite SiC, gold and the limiting case of MWAs by calculating $\mathrm{Im}[r_{TM}]\exp(-\gamma d)$. The LDOS of MWAs is largely enhanced in a broad frequency band

compared to that of gold. The LDOS of SiC has a sharp peak at the SPR frequency. The LDOS of MWAs as shown in Fig. 2 is almost evenly distributed in the infrared regime. Hence, MWAs can strongly interact with an IR-SPR emitter (e.g., SiC) and simultaneously maintain the monochromatic near-field heat transfer with the IR-SPR emitter, according to Eq. (4).

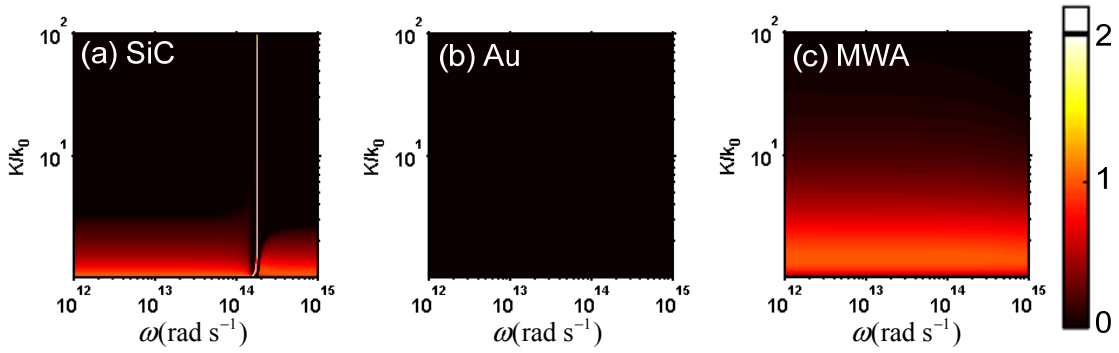

FIG. 2: (color online). Plot of the expression $\mathrm{Im}[r_{TM}]\exp(-\gamma d)$ to estimate the photon local density of state (LDOS) at $d = 100$nm above the surface of semi-infinite (a) SiC, (b) Au, and (c) limiting case of metal wire arrays (MWAs).

III. Wiener-chaos expansion method

Since conventional approaches for directly calculating near-field radiation mainly rely on the analytical forms of dyadic Green functions[25], these calculations can only be conducted for simple geometries: e.g., semi-infinite plates, spheres and multi-layers. For complex structures such as metamaterials, EMT is often employed to approximate the arrays of inhomogeneous sub-wavelength structures as a homogenous medium with effective electric and magnetic properties. There exist few direct numerical methods to simulate near-field radiation. Guérout *et al.*[26] developed a method based on scattering theory to calculate the radiative heat transfer between one-dimensional gratings. Rodriguez *et al.* [27] conducted a direct simulation to investigate the near-field radiative heat transfer between two photonic crystal slabs using the Monte Carlo method. Very recently, Rodriguez *et al.*[28] proposed a fluctuating surface-current (FSC) formulation to evaluate radiative heat transfer for arbitrary geometries based on the boundary element method (BEM). Badieirostami[29] and Wen[30] conducted non-stochastic direct simulations for incoherent light sources and radiative heat transfer between two parallel plates, respectively, based on the Wiener-chaos expansion method. Here, we perform a direct numerical simulation of near-field radiation for complex three-dimensional geometries (e.g., MWAs) using the Wiener-chaos expansion method[29,30] by finite-difference time-domain (FDTD) technique.

The unique properties of the Wiener-chaos expansion method are summarized below. First, unlike the scattering theory formulations described in Ref. [26], the Wiener-chaos expansion method does not require any modes expansion over wave vector. It only relies on finding a proper orthonormal basis of the geometries. Thus, the Wiener-chaos expansion method can be used to calculate the thermal radiation from arbitrary geometries. Second, the Wiener-chaos expansion method is a non-stochastic method and it does not need any random number generators, whereas a proper random number generator is critical for the efficiency and accuracy of the Monte Carlo method[29]. Furthermore, the Wiener-chaos expansion method can be implemented by the standard FDTD technique, which can obtain the spectrum information (i.e., spectral energy flux from each mode) from a single simulation. However, the data points at different frequencies need to be simulated separately by the frequency-domain methods, such as the FSC method[28] and the finite-difference frequency-domain implementation of the Wiener-chaos expansion method in Ref. [30].

Thermal radiation from an object physically originates from thermally induced random currents $J_{\mathbf{l}}(r,\omega)$ whose mean value is equal to zero. According to fluctuation electrodynamics[31], the thermally induced random currents are spatially and temporally incoherent, which satisfy

$$\left\langle J_{\mathbf{k}}(r,\omega)J_{\mathbf{l}}^{*}(r',\omega')\right\rangle = V(\omega,T)^2\,\delta(\omega-\omega')\delta_{\mathbf{kl}}\delta(r-r'), \quad (5)$$

where $V(\omega,T)=\sqrt{4\varepsilon_0\,\mathrm{Im}[\varepsilon_r]\Theta(\omega,T)/\pi}$ is a deterministic function, the bracket $\langle\cdot\rangle$ denotes the statistical ensemble average, ε_0 is the permittivity of vacuum, $\mathrm{Im}[\varepsilon_r]$ is the imaginary part of the dielectric function of the object, and $\Theta(\omega,T)=\hbar\omega/[\exp(\hbar\omega/k_BT)-1]$ is the Planck distribution. $\delta_{\mathbf{kl}}\delta(r-r')$ are the Kronecker delta and Dirac delta functions that indicate the random currents are incoherent at different polarization ($\mathbf{l}$ and $\mathbf{k}$) and different locations, respectively. $\delta(\omega-\omega')$ indicates the temporal incoherence. Due to the spatial incoherence, $J_{\mathbf{l}}(r,\omega)$ at a certain frequency can be constructed as $J_{\mathbf{l}}(r,\omega)=V(\omega,T)dW(r)\mathbf{l}$, where $dW(r)$ is the white noise function (i.e., the derivative of Brownian motion) that has the properties $\langle dW(r)\rangle=0$ and $\langle dW(r)dW(r')\rangle=\delta(r-r')$. $dW(r)$ has been extensively studied in stochastic process theories and can be expanded by the Karhunen-Loève expansion as $dW(r)=\sum_{n=1}^{\infty}c_nf_n(r)$ [32], where $\{f_n\}$ is an orthonormal basis for a volume S with thermal sources defined by $\int_{r\in S}f_i(r)f_j^*(r)d^3r=\delta_{ij}$, and c_n are the uncorrelated random variables satisfying $\langle c_i\rangle=0$, $\langle c_ic_j\rangle=\delta_{ij}$. Thus, the random current sources can be expanded as the linear combination of the orthogonal *current modes* $\{j_n(r,\omega)=V(\omega,T)f_n(r)\}$, such that $J_{\mathbf{l}}(\omega,r)=\sum_{n=1}^{\infty}c_nj_n(r,\omega)\mathbf{l}$. Now Eq. (5) can be rewritten as

$$\left\langle J_1(r,\omega)J_1^*(r',\omega)\right\rangle = \sum_{n=1}^{\infty}\sum_{m=1}^{\infty}\left\langle c_n c_m \right\rangle j_n(r,\omega)j_m^*(r',\omega). \qquad (6)$$
$$= \sum_{n=1}^{\infty} j_n(r,\omega)j_n^*(r',\omega)$$

According to Maxwell's equations, energy flux $q(\omega)$ is usually related to the current source term $J(r,\omega)J^*(r',\omega)$ by a linear operator $L[\cdot]$ as $q(\omega) = L[J(r,\omega)J^*(r',\omega)]$ [1,2]. Here, $L[\cdot]$ is the standard dyadic Green function, which is the electromagnetic response to a point dipole source. From Eq. (6) the average energy flux from the random currents $\langle q(\omega)\rangle = L[\langle J(r,\omega)J^*(r',\omega)\rangle]$ can be expanded as the sum of the energy flux from each current mode $q_n(\omega) = L[j_n(r,\omega)j_n^*(r',\omega)]$:

$$\langle q(\omega)\rangle = L[\langle J(r,\omega)J^*(r',\omega)\rangle]$$
$$= \sum_{n=1}^{\infty} L[j_n(r,\omega)j_n^*(r',\omega)], \qquad (7)$$
$$= \sum_{n=1}^{\infty} q_n$$

which is illustrated in Fig. 3.

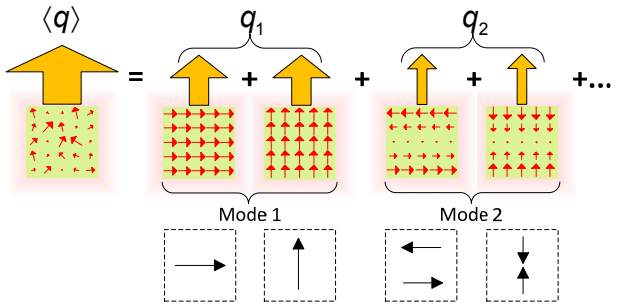

FIG. 3: (color online). Average energy flux radiated from random current sources is expanded as the sum of the energy flux from each orthogonal current mode. Fast convergence can be achieved when the current modes are chosen in sinusoidal forms.

The primary challenge of the Wiener-chaos expansion method is to find proper current modes of thermal sources. For instance, when the current modes are chosen in sinusoidal forms, their expansion can be physically viewed as classical multipole expansion (Fig. 3), which leads to fast convergence for energy flux calculation[33]. Hence we can truncate the expansion and only keep the lower order current modes without losing accuracy. For complicated geometries, the current modes can be generated in spherical harmonic forms using the algorithms developed in Ref. [34].

IV. Simulation results

Here, we investigate the near-field radiative heat transfer between an IR-SPR emitter and MWAs placed in vacuum. The IR-SPR emitter is assumed to be a $1\mu m$ thick plate. Metal wires are aligned in the z-direction with radius r =50nm and period a =300nm. The IR-SPR emitter is kept at 300K, and the MWAs are at 0K. The heat flux between them is evaluated by calculating the amount of energy transmitted into the MWAs. As the MWAs are at a finite temperature, the net heat flux can be solved by the reciprocity of radiative heat transfer[27]. In our simulation, the current modes in the IR-SPR emitter are chosen in sinusoidal forms (see Appendix) because of the resulting high convergence speed of numerical simulation. The MWAs at 0K do not emit thermal radiation, and we only consider their electromagnetic response in the infrared range. The metal wires in our simulation are assumed to be PEC wires, which is verified by comparing the energy fluxes into PEC and gold wire arrays for current *Mode 1*. We find that the results from PEC and gold wires are almost the same, as shown in Fig. 4.

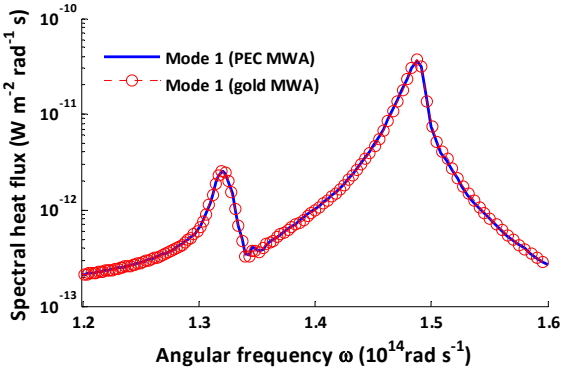

FIG. 4: Spectral heat flux into PEC MWA and gold MWA due to current Mode 1. The MWAs have the same geometry: wires radius $r = 50$nm, wires period $a = 300$nm. The vacuum gap size d between the MWAs and SiC plate is 100nm.

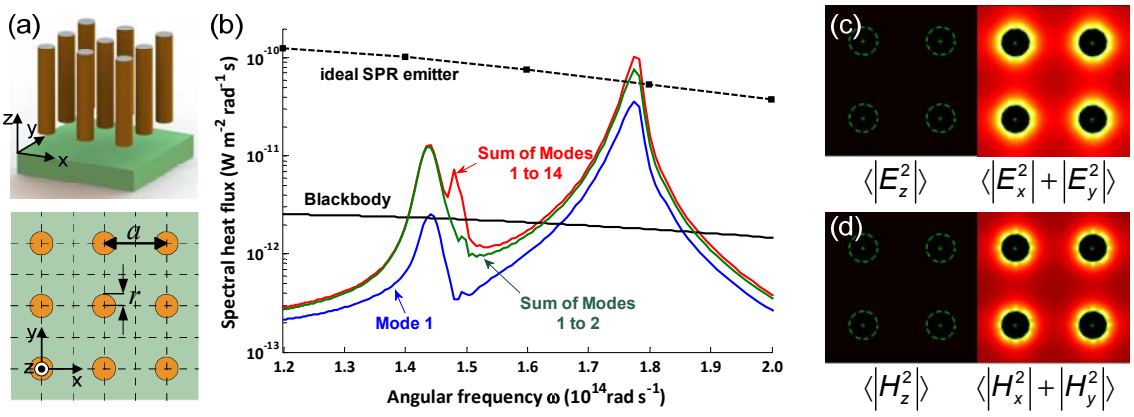

FIG. 5: (color online). (a): Schematic diagram (3D view and top view) of the SiC plate heat emitter (at 300K) and the metal wire arrays heat absorber (at 0K) separated by a vacuum gap. Metal wires have infinite length, radius r =50nm and period a =300nm. (b) Spectral heat flux into metal wire arrays from sinusoidal current modes in the SiC plate at a 100nm vacuum gap. (c), (d) Electric and magnetic field profiles in metal wire arrays at the SPR frequency (1.78×10^{14} rad/s) of SiC, measured at the plane $2\mu m$ above the gap.

The spectral heat flux between a SiC emitter and the MWAs with a 100nm gap is plotted in Fig. 5(b). The first current mode (dipole-like mode) contributes $\approx 40\%$ of the total heat flux, and the first two modes contribute $\approx 80\%$. The monochromatic feature of heat transfer is denoted by the peaks corresponding to the symmetric and antisymmetric SPR modes of the $1\mu m$ thick SiC plate, where near-field heat transfer clearly exceeds the Planck law. The broadband response from the MWAs can be found by introducing an "ideal SPR emitter" that has a frequency-independent permittivity equal to $-1+bi$. The real part, -1, indicates that the material supports SPR at any frequency, and the imaginary part b is an arbitrary number associated with the magnitude of thermal induced currents in Eq. (5). In Fig. 5(b), b is assumed to be 0.1. The spectral heat flux between the "ideal SPR emitter" and the MWAs is plotted in Fig. 5(b). Heat transfer enhancement is observed for all the frequencies of interest in the infrared regime.

The mechanism with which MWAs absorb heat is directly elucidated in our simulations. The field profiles inside the MWAs at the SPR frequency of SiC are shown in Fig. 5(c) and (d). The highly spatial dispersion of MWAs leads to the TEM (transverse electromagnetic, $E_z = H_z = 0$) propagating modes[18]. At the frequencies below the equivalent plasma frequency ω_p, the hyperbolic dispersion relation becomes flat as $k_z^2 = k_0^2$. Thus, the MWAs support the TM waves with arbitrary K propagating only along the z direction (i.e., TEM waves)[19]. For real MWAs (e.g., gold wire arrays),

they couple the TM waves (both propagating and evanescent components) from the IR-SPR emitter into the TEM waves propagating along the wires, which will eventually be absorbed by metals due to the ohmic loss. In the frequency range of thermal radiation, the MWAs can be viewed as a system of coupled low-loss transmission lines[18]. The decay length L_d of the gold wires in Fig. 5 is estimated to be on the order of 100 μm by the approach described in Ref. [19] that $L_d \approx Im[k_z]^{-1}$ for the TEM waves with $K = 0$. With this low-loss feature, MWAs can also be used as "near-field thermal waveguides" which can couple the evanescent radiative energy at the nanoscale and transfer it to a macroscopic scale.

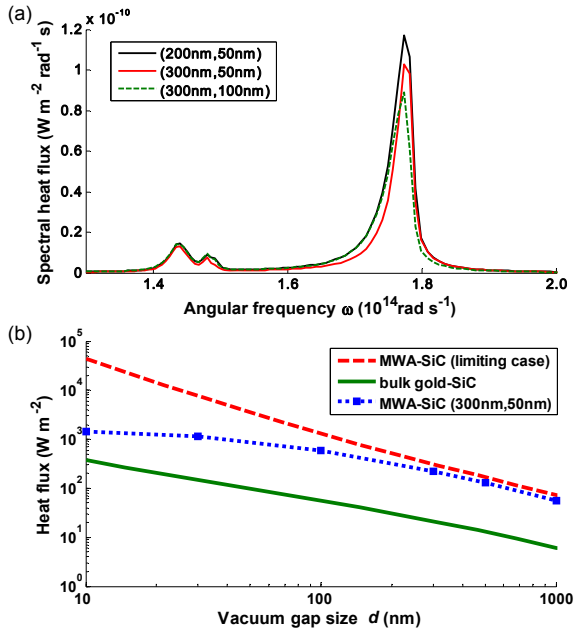

FIG.6: (color online). (a) Comparison between heat fluxes from $1\mu m$ thick SiC plate (at 300K) to MWAs (at 0K) and semi-infinite gold plate (at 0K), as a function of the vacuum gap size. Also the performance of ideal MWAs is plotted for reference. (b) Spectral heat flux between the SiC plate and the MWAs with different (a, r) at a 100nm gap. Here a, r denote the period and the radius of metal wires, respectively.

In Fig. 6(a), we plot the total heat flux between the SiC IR-SPR emitter and the MWAs against gap sizes. Compared with the SiC-gold case, MWAs can enhance the near-field heat transfer with SiC by one order of magnitude without having to match the SPR in SiC. These results show that MWAs significantly modify the radiative thermal properties of bulk metals in the near-field. For a fixed gap, the performance of MWAs is determined by wire density and size. As shown in Fig. 5(c) and (d), the transmitted energy in the MWAs is concentrated on the surface of each wire. MWAs with

smaller radii and periods are expected to absorb more energy. This trend is demonstrated by calculating the spectral heat fluxes to MWAs with different wire radii and periods (Fig. 6(b)). The performance of MWAs can be maximized when the period of the wires is infinitely small, which is the limiting case presented in Sec. II. The radiative heat transfer between this limiting case of MWAs and a SiC emitter can be calculated analytically by modeling the MWAs as an anisotropic medium with local dispersion relation based on EMT[16,35], as shown in Fig. 6(a). At large gaps, the limiting case EMT approximation gives an accurate prediction. However, for small gaps, it overestimates the heat transfer in actual cases. Therefore, a direct numerical simulation is required to accurately predict the performance.

V. Conclusion

In this paper, we described a hyperbolic metamaterial based heat emitter/absorber made of metal wire arrays (MWAs), which can greatly enhance near-field heat transfer with IR-SPR materials. Rather than match the resonant frequencies of IR-SPR materials, MWAs are non-resonant and have enormous enhancement of the LDOS in a broad frequency range. We directly simulated the near-field radiative heat transfer between MWAs and an IR-SPR emitter based on the Wiener-chaos expansion method. The direct numerical simulation is demonstrated to be critical for accurately predicting the near-field radiation of complex geometries like metamaterials. Manipulation of near-field radiation using metamaterials has been considered in theory for a long time but is difficult to be experimentally realized. The results presented in this paper provide a feasible way to achieve the metamaterials which can work in the near-field and enhance radiative heat transfer beyond material limitation.

Acknowledgments

This work is supported by the National Science Foundation (CBET-1253692). The authors would also like to thank Jean-Jacques Greffet for the valuable discussion during ASME 2012 3rd Micro/Nanoscale Heat & Mass Transfer International Conference.

Appendix: Current Modes

As discussed in Sec. III, a proper set of current modes in thermal emitters $\{j_i(r) = V(\omega,T) f_i(r)\}$ can be selected by choosing a set of orthonormal basis functions $\{f_i\}$ in sinusoidal forms. When dealing with the periodic structures such as metamaterials, the quality of the current modes can be further improved by taking advantage of the periodicity and symmetry of the geometries.

In the simulation of the heat transfer between the IR-SPR emitter and MWAs, as shown in Fig. 5(a), the orthonormal basis $\{f_i\}$ is defined in the volume of the 1 μm-thick SiC plate. Since the

structure is periodic in x,y direction, the infinite plate can be divided into cuboid cells with a height of $h = 1\mu m$ and a length and a depth of $a/2$. Thus, the orthonormal basis $\{f_i\}$ for this infinite plate can be chosen as the union of the orthonormal basis for all the cuboid cells. Consider the cuboid cell centered at $(x_c, y_c) = \left(\frac{a}{4}[2c_x + 1], \frac{a}{4}[2c_y + 1]\right)$, where c_x and c_y are integers. The orthonormal basis for this cell is chosen as the Fourier-series basis $\{f_{l,m,n,\mathbf{k},c_x,c_y}\}$, where

$$f_{l,m,n,\mathbf{k},c_x,c_y}(x,y,z) = H_l(x - x_c)\cdot P_m(y - y_c)\cdot G_n(z + h)\mathbf{k}\,, \qquad \text{(A8)}$$

and

$$H_l(x) = \begin{cases} \sqrt{\frac{2}{a}} & l = 0 \\ \sqrt{\frac{4}{a}}\cos\left[\frac{l\pi(x + c_x a/2)}{a/2}\right] & l = 1,2,3... \end{cases}$$

$$P_m(y) = \begin{cases} \sqrt{\frac{2}{a}} & m = 0 \\ \sqrt{\frac{4}{a}}\cos\left[\frac{m\pi(y + c_y a/2)}{a/2}\right] & m = 1,2,3... \end{cases} . \qquad \text{(A9)}$$

$$G_n(z) = \begin{cases} \frac{1}{\sqrt{h}} & n = 0 \\ \sqrt{\frac{2}{h}}\cos\left[\frac{n\pi z}{h}\right] & n = 1,2,3... \end{cases}$$

Here, $x - x_c, y - y_c \in [-a/4, a/4]$, $z \in [-h, 0]$, $\mathbf{k} \in \{\mathbf{e_x}, \mathbf{e_y}, \mathbf{e_z}\}$ is the unit vector of 3D space. Then the current modes in the SiC plate become $\{j_{l,m,n,\mathbf{k},c_x,c_y}(r,\omega) = V(\omega,T) f_{l,m,n,\mathbf{k},c_x,c_y}(r)\}$.

Due to the periodicity and symmetry of the structure, the current modes in different cuboid cells have the same contribution to thermal radiation. Therefore, we only need to evaluate the current modes in one cell, which can be chosen as $c_x = c_y = 0$. Since the current modes in sinusoidal forms can be viewed as a multipole expansion, they can be divided into different groups with ranking numbers, which are similar to the orders in the multipole expansion. The top 14 groups of current modes are listed in Table I. For example, *Mode 1* denotes the group of current modes $\{j_{l,m,n,\mathbf{k},c_x,c_y}\}$ with $l = m = n = 0$. It can be viewed as the term of dipole approximation, which is similar to the concept mentioned in Ref. [36].

Mode ranking	l	m	n
1	0	0	0
2	0	0	1
3	0	0	2
4	0	0	3
5	0	0	4
6	0	0	5
7	0	1	0
8	1	0	0
9	0	1	1
10	1	0	1
11	0	1	2
12	1	0	2
13	1	1	0
14	1	1	1

TABLE I: The ranking of the groups of the current modes mentioned in Sec. IV.

Reference

[1] K. Joulain, J.-P. Mulet, F. Marquier, R. Carminati, and J.-J. Greffet, Surf. Sci. Rep. **57**, 59 (2005).

[2] A. Volokitin and B. Persson, Rev. Mod. Phys. **79**, 1291 (2007).

[3] V.P. Carey, G. Chen, C. Grigoropoulos, M. Kaviany, and A. Majumdar, Nanoscale and Microscale Thermophysical Engineering **12**, 1 (2008).

[4] J.-P. Mulet, K. Joulain, R. Carminati, and J.-J. Greffet, Microscale Therm. Eng. **6**, 209 (2002).

[5] E. Rousseau, A. Siria, G. Jourdan, S. Volz, F. Comin, J. Chevrier, and J.-J. Greffet, Nat. Photon. **3**, 514 (2009).

[6] S. Shen, A. Narayanaswamy, and G. Chen, Nano Lett. **9**, 2909 (2009).

[7] C.J. Fu and Z.M. Zhang, Int. J. of Heat Mass Trans. **49**, 1703 (2006).

[8] S.-A. Biehs, E. Rousseau, and J.-J. Greffet, Phys. Rev. Lett. **105**, 234301 (2010).

[9] S. Basu, Z.M. Zhang, and C.J. Fu, Int. J. Energ. Res. **33**, 1203 (2009).

[10] A. Narayanaswamy and G. Chen, Appl. Phys. Lett. **82**, 3544 (2003).

[11] C.R. Otey, W.T. Lau, and S. Fan, Phys. Rev. Lett. **104**, 154301 (2010).

[12] S. Basu and M. Francoeur, Appl. Phys. Lett. **98**, 113106 (2011).

[13] K. Joulain and J. Drevillon, Phys. Rev. B **81**, 165119 (2010).

[14] Y. Liu and X. Zhang, Chem. Soc. Rev. **40**, 2494 (2011).

[15] W. Cai and V. Shalaev, *Optical Metamaterials: Fundamentals and Applications* (Springer, 2010).

[16] S.-A. Biehs, P. Ben-Abdallah, F.S.S. Rosa, K. Joulain, and J.-J. Greffet, Opt. Express **19**, A1088 (2011).

[17] J.B. Pendry, Opt. Photon. News **15**, 32 (2004).

[18] P.A. Belov, R. Marqués, S.I. Maslovski, I.S. Nefedov, M. Silveirinha, C.R. Simovski, and S.A. Tretyakov, Phys. Rev. B **67**, 113103 (2003).

[19] G. Shvets, S. Trendafilov, J.B. Pendry, and A. Sarychev, Phys. Rev. Lett. **99**, 053903 (2007).

[20] S. Basu and M. Francoeur, Appl. Phys. Lett. **99**, 143107 (2011).

[21] S.-A. Biehs, M. Tschikin, and P. Ben-Abdallah, Phys. Rev. Lett. **109**, 104301 (2012).

[22] J.B. Pendry, A. Holden, W. Stewart, and I. Youngs, Phys. Rev. Lett. **76**, 4773 (1996).

[23] J.B. Pendry, J. Phys.: Condens. Matter **11**, 6621 (1999).

[24] G.S. Agarwal, D.N. Pattanayak, and E. Wolf, Phys. Rev. B **10**, 1447 (1974).

[25] D. Polder and M. Van Hove, Phys. Rev. B **4**, 3303 (1971).

[26] R. Guérout, J. Lussange, F. Rosa, J.-P. Hugonin, D. Dalvit, J.-J. Greffet, A. Lambrecht, and S. Reynaud, Phys. Rev. B **85**, 180301 (2012).

[27] A. Rodriguez, O. Ilic, P. Bermel, I. Celanovic, J. Joannopoulos, M. Soljačić, and S. Johnson, Phys. Rev. Lett. **107**, 114302 (2011).

[28] A. Rodriguez, M. Reid, and S. Johnson, Phys. Rev. B **86**, 220302 (2012).

[29] M. Badieirostami, A. Adibi, H. Zhou, and S. Chow, Multiscale Model. Simul. **8**, 591 (2010).

[30] S.-B. Wen, Journal of Heat Transfer **132**, 072704 (2010).

[31] S.M. Rytov, Y.A. Kravtsov, and V.I. Tatarskii, *Principles of Statistical Radiophysics*, Vol. 3. (Springer-Verlag, 1989).

[32] D. Xiu, *Numerical Methods for Stochastic Computations: a spectral method approach* (Princeton Unversity Press, 2010).

[33] P.C. Chaumet, A. Rahmani, F. de Fornel, and J.-P. Dufour, Phys. Rev. B **58**, 2310 (1998).

[34] M.K. Chung, A. Qiu, and M. Nacewicz, in *2nd MICCAI Workshop on MFCA* (2008).

[35] P. Ben-Abdallah, K. Joulain, J. Drevillon, and G. Domingues, J. Appl. Phys. **106**, 044306 (2009).

[36] J.-P. Mulet, K. Joulain, R. Carminati, and J.-J. Greffet, Appl. Phys. Lett. **78**, 2931 (2001).